 doi:10.20944/preprints202005.0088.v1

Steric Blockage of Lysenin Toxin by Crowding

Ignacio L.B. Munguira[1] & Alfonso Barbas[2]

[1] U1006 INSERM, Université Aix-Marseille, Parc Scientifique et Technologique de Luminy, 163 avenue de Luminy, 13009 Marseille, France
[2]Instituto de Fusión nuclear, José Gutiérrez Abascal 2, 28006 Madrid, Spain

Abstract

Increasing evidence signals the importance of macromolecular crowding on the regulation of the membrane protein activity. Lysenin is a pore forming toxin that forms crowded assemblies in membrane containing sphingomyelin microdomains. We studied the role of crowding on the activity of Lysenin thanks to High Speed Atomic Force Microscopy. In this study we show that pore formation requires available space around to take place, being sterically block in crowded environments, and verified it with non-Supported Lipid Bilayers mimicking the mechanical conditions of cell membranes. A continuous pH decrease and a single molecule compression experiments show that pore formation liberates membrane space leading to prepore-to-pore transitions. The study of the effects of prepore insertion comparing pore formation induced by sudden pH decrease in lysenin assemblies with thousand simulations show that liberation of space unblocks pore formation and could contribute to elude the cellular non-immune defences. Based on our findings we propose a refinement of current prepore structure and insertion models. We envision novel antibiotic strategies based on toxin-binding-domains “crowders”.

Keywords: Pore Forming Toxins, crowding, prepore-to-pore transition

Preprints (www.preprints.org) | NOT PEER-REVIEWED | Posted: 5 May 2020 doi:10.20944/preprints202005.0088.v1

Introduction

Macromolecular crowding comprises the effects of macromolecules on itselfs in a high volume fraction of them[1]. In early 2000s, the role of macromolecular crowding in biomolecular processes was still underappreciated[2]. Nowadays, macromolecular crowding has been identified as a biologically significant factor both in cytoplasm and membrane. There is clear evidence of the role of crowding in the regulation on the gene expression[3], on the gating energies of membrane proteins[4], and on the membrane protein conformational landscape [5,6]. As factors incorporated to the already crowded membranes, Pore Forming Toxins (PFTs)[7] are emerging as important elements to reproduce crowding conditions *in vitro*, allowing to study crowding effects[8,9,10]. PFTs are known to bind as monomers to lipid raft-like domains to boost monomer density to increase the oligomerization efficiency[11,12]. Being the PFTs naturally inclined to crowding, they should be adapted to develop their functions on crowded environments. In the present work we investigate crowding as a regulation factor for lysenin.

Lysenin[13] is emerging as a model system for PFT studies and crowding[14,15,10]. Lysenin molecular mechanism starts with a soluble monomer which binds pentamerically to sphingomyelin (SM) clusters[8] , where it assembles into nonameric oligomers known as prepores[10]. The cholesterol (Chol) also present in the cluster facilitates Lysenin oligomerization[16].Prepore insertion entails a large structural change, triggered by pH and calcium change[17], which results in the so-called pore state. The structure of the lysenin pore is known with atomic resolution[18], however the structure of the prepore was never determined with such a detail. The only available data about the lysenin prepore structure was obtained by HS-AFM[14], and suggests prepore-pore diameter difference of 3 Å; 5.5 nm^2 in occupied area[18]. The prepore model impose the same prepore-pore diameter[18,19], further work in lysenin crowded assemblies can help to develop a more accurate prepore model. A new model of prepore structure and prepore-to-pore transition is required to better understand electrophysiology experiments[9] and vesicle permeabilization[20] that point towards a congestion of pore state of lysenin in crowding conditions. Proof of a role of crowding in the action of PFTs is still missing, probably due to the lack of a suitable technique to correlate local crowding to PFT structure. High Speed Atomic Force Microscopy (HS-AFM)[21] has brought new possibilities to study toxins dynamics and it is the adequate technique to study crowding effects in membranes, providing on unlabelled molecules, sub-second temporal resolution and full visualization of the molecular nanoenvironment[10 14 15].

Preprints (www.preprints.org) | NOT PEER-REVIEWED | Posted: 5 May 2020 doi:10.20944/preprints202005.0088.v1

Methods

Lysenin from earthworm Eisenia foetida was obtained from Peptide Institute (Osaka, Japan), and rehydrated with Phosphate-buffered saline (PBS) at pH 7.5 to reach a final concentrations of 1.6 and 5.0 µM. Egg Sphingomyelin (SM) and Cholesterol (chol) (Avanti Polar Lipids, Alabama, USA) at a molar ratio SM/Chol (1:1) were used to form small unilamellar vesicles (SUVs) and giant unilamellar vesicles (GUVs). To form the supported lipid bilayers (SLBs), 1 µl of SUV or GUV solution was placed on a 1.5 mm-diameter freshly cleaved mica disk covered with 1 µl of Phosphate-buffered saline (PBS) and incubated for 30 minutes. Once the bilayer was formed, 1 µl of 1.6 or 5.0 µM. Lysenin solution was incubated for 15 minutes. HS-AFM observations were performed in oscillating mode using optimized high-resolution imaging parameters[32]. Short cantilevers designed for HS-AFM with a length of ~8 µm, a spring constant of 0.1–0.2 N m^{-1}, a resonance frequency of 600 kHz and a quality factor of ~2 in solution were used, bearing an electron beam deposition tip at the end of the cantilever. The sensitivity of the AFM system to probe deflection was 0.1 V nm^{-1}. The free amplitude was ~10 Å and the imaging amplitude setpoint was set to ~90% of the free amplitude. Under such conditions, the force applied by the HS-AFM tip on the sample was estimated to be < 100 pN. Controlled force AFM observations were performed on a multimode-V microscope from Bruker Corporation, Santa Barbara, CA in PeakForce mode. PEAKFORCE-HIRS-SSB model cantilevers with a spring constant of 0.1 N m^{-1} were used.

Results and discussion

Here we used assemblies of lysenin prepores and pores on supported lipid bilayers (SLB) composed of SM/Chol 1:1, to mimicking lipid raft domains composition[22]. First, we screened different monomer incubation concentrations. Remarkably, these incubations revealed that the incubation concentration directly affects the percentage of pores present in the ensemble. We focused on two incubation concentrations, a monomer concentration at 1.6 µM, where the pore state was predominant, being 78±2% of the total number of oligomers (**Fig. 1a**), and a monomer concentration at 5.6µM, where the pore state was in minority with 13±4% of pores (**Fig. 1b**). As the pore state is more abundant at lower levels of crowding and less at higher levels of crowding, where the prepore state is more abundant, we concluded that the prepore-to-pore transition got blocked at higher levels of crowding. This finding suggested that the prepore-to-pore transition required the presence of available space around the toxin prepores, or otherwise the prepore-to-pore transition got sterically inhibited. We also found that the incubation concentration affected the supramolecular organization on the membrane. Incubations at a concentration of 1.6µM resulted in clusters of lysenin pores surrounded by protein-free membrane areas (**Fig. 1a**), whereas incubations at 5.6µM resulted in hexagonal close packed (hcp) assemblies composed mainly of lysenin prepores (**Fig. 1b**). The negative hydrophobic mismatch of the β-barrels of the lysenin pores is the probable cause of the observed attraction between pores (details on Supplementary section).

Preprints (www.preprints.org) | NOT PEER-REVIEWED | Posted: 5 May 2020 doi:10.20944/preprints202005.0088.v1

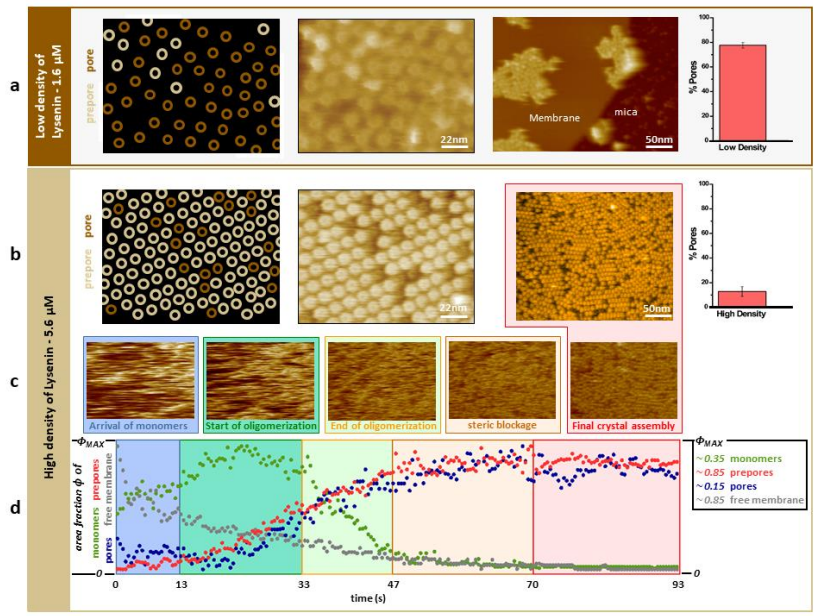

Figure 1. The incubation concentration of lysenin in the SM/Chol 1:1 membranes determine prepore/pore populations. *At low concentration incubation (1.6µM lysenin, 15min)*: **a**, the lysenin oligomers form amorphous aggregates in the SM/Chol 1:1 bilayer, HS-AFM images. 78±2% of the lysenin oligomers are in the pore state. Error bar is the standard deviation of five experiments. *At high concentration incubation (5.0µM lysenin, 15min)*: **b**, the lysenin oligomers form hexagonal-closed packed assemblies, with a 13±4% of the lysenin oligomers are in the pore state. Error bar is the standard deviation of five experiments. **c**, HS-AFM images of the five stages identified during the filling of the membrane by lysenin at high concentration. **d**, Lysenin oligomerization process. To identify when the steric inhibition occurs we film the molecular mechanism of lysenin from the initial binding of monomers to the formation of the 2D crystal. We identify four types of sample under the pixel by its pixel-height (free membrane, monomers, prepores and pores), we measure the area fraction of each of these populations. We find five different milestones during the filling of the membrane, by order of appearance we find; the arrival of monomers (with a maximum in the free membrane area), the start of oligomerization (when the area of prepores and pores start to increase, indicating the start of oligomerization, but the area of monomer remains high), the end of oligomerization (characterize by a gradual increase of the areas of prepores and pores link with the decrease to the minimum of the free membrane and monomers areas), the steric blockage (where all areas start to stabilize), and the reach of the final 2D crystalline assembly. Contrarily to what could be expected for pore-forming toxins the prepore state is not followed by the insertion in the membrane, the prepore-to-pore transition gets blocked over a certain level of crowding.

To exclude uncontrolled effects derived from the presence of the mica substrate below the membrane[1], we repeated the high concentration incubation on non-supported lipid bilayers (nSLB)[23] of SM/Chol 1:1. The imposition of a flat surface to the membrane or the anchoring of individual lysenin oligomers[10] could affect previous observations. The use of nSLB mimics the curvature and tension of the native environment of membranes in cells, and anchoring of oligomers is excluded[14]. The 5.6µM incubation on nSLB, with a 78% of lysenin oligomers in the prepore state, confirmed that the prepore state is dominant regardless of the substrate, the membrane tension or the curvature (**Suppl. Fig. 1**). The results on nSLB suggest that the steric inhibition is a general phenomenon of the crowded assemblies of lysenin.

Preprints (www.preprints.org) | NOT PEER-REVIEWED | Posted: 5 May 2020 doi:10.20944/preprints202005.0088.v1

To get further insight on the phenomenon of prepore-to-pore transition steric inhibition in lysenin toxin, we filmed at 0.45 seconds per frame the evolution of a SM:Chol 1:1 membrane exposed to lysenin monomers solution (**Fig. 1d, Suppl. movie 1**). We time-tracked changes in the occupancy of the membrane by monomers, prepores and pores. A pixel height count methodology was used in order to localize each population (details on Methods section). We evidenced a sequence of events that lead to steric inhibition, with five stages in the filling of the membrane (**Fig. 1c**). First, the arrival of lysenin monomers (**Fig. 1d**, t<13 s, in blue). Second, the beginning of oligomerization (**Fig. 1d**, t~25 s, in green). Third stage, where most of the oligomerizations took place, in which we observed an abrupt decrease on the lysenin-free membrane area lead by monomer membrane occupancy. This stage, called oligomerization end, finish with an almost full coverage of membrane with lysenin oligomers (**Fig. 1d**, t<47 s, in pale green). Fourth, the steric blockage of prepore insertions, where the number of prepores and pores remained constant (**Fig. 1d**, t<70 s, orange). At this stage with a vast majority of Lysenin oligomers in the prepore stage where we think that the prepore-to-pore transition got sterically blocked. Moreover, at that time the oligomer assembly exhibited certain degree of dynamism. For tens of seconds the oligomers searched for a stable state until every oligomer position got fixed in the last stage, the 2D crystal assembly (**Fig. 1d**, t>70 s, red). We note that this time series represents one of the few data sets showing the process of 2D protein crystal growth[24].

How did lysenin evolutionary overcome the steric blockage on the prepore-to-pore transition owing its ability to form pores?[25]. We first want to check if as suggested by *Podobnik et al*.[18] data, prepore-to-pore transition liberate space. Following previous results in which a pH-decrease induced prepore-to-pore transitions in lysenin 2D prepore assemblies[17], we induce new insertions and measured the occupy area by each population. We decided to use a membrane patch sufficiently small to be fully visualized by the HS-AFM. Previous HS-AFM works on lysenin were performed on large membrane patches where local effects could be hidden out of visualized area[10 14 15 17]. A small SM/Chol 1:1 patch (around 600nm in diameter) we performed 5.6µM lysenin incubation inducing the full filling of the patch. We counted ~315 lysenin oligomers, out of which 95% were in prepore state. We induced the prepore-to-pore transition by a continuous pH decrease from 7.5 to 5.2 inducing ~135 insertions, 43% of all prepores (**Fig. 2a**,**b** and **suppl. movie 2**). Along with the induced insertions we observed a decrease of the membrane area occupied by lysenin oligomers of ~16%. Thanks to this results we check directly a membrane occupancy reduction by Lysenin oligomers induced by the prepore-to-pore transition. The prepore and prepore-to-pore transition models should, as previously suggested[19], be modify to adequate our findings. Following our results the superimposition of lysenin monomeric structure on C-terminal domains of the pore structure that impose the shame pore and prepore diameter is not correct. Interestingly, the total area of the patch remained invariant during the insertions, this was combined with the appearance of seemly lipid protrusions on top of the pores (**Suppl. Fig. 2**). The lysenin seemly punches the membrane during the pore formation. This type of mechanism was recently identified in the suilysin toxin[26].

Preprints (www.preprints.org) | NOT PEER-REVIEWED | Posted: 5 May 2020 doi:10.20944/preprints202005.0088.v1

In order to discard any possible electrostatic effect of pH change on the appearance of protein-free membrane area, we induced prepore insertions using single molecule compressions[27]. We performed force mapping experiments at constant pH of 7.5 in hcp lysenin assemblies presenting 94% of prepores. We imaged a 50x50 nm area where we increased the applied force of the AFM imaging from 300pN to 600pN. As a result, prepore-to-pore transitions were induced (**Fig. 2c**). Visualizing the area after a zoom out at 300pN forces, more than half of the formed pores presented lateral displacements >1nm with respect their previous positions (**Fig. 2c**). All the lysenin that remained in prepore state stay in the same position. We concluded that the insertion of lysenin is related to the liberation of certain membrane space. The motion of the pores formed by AFM compression from their initial positions confirms the findings by pH-decrease. Biologically, this liberation of space could be the answer found by lysenin to confront the necessity of crowded environments to enhance oligomerization with the necessity of scape steric inhibitions. Remarkably, all new pores appear to form clusters with no pore surrounded just by prepores.

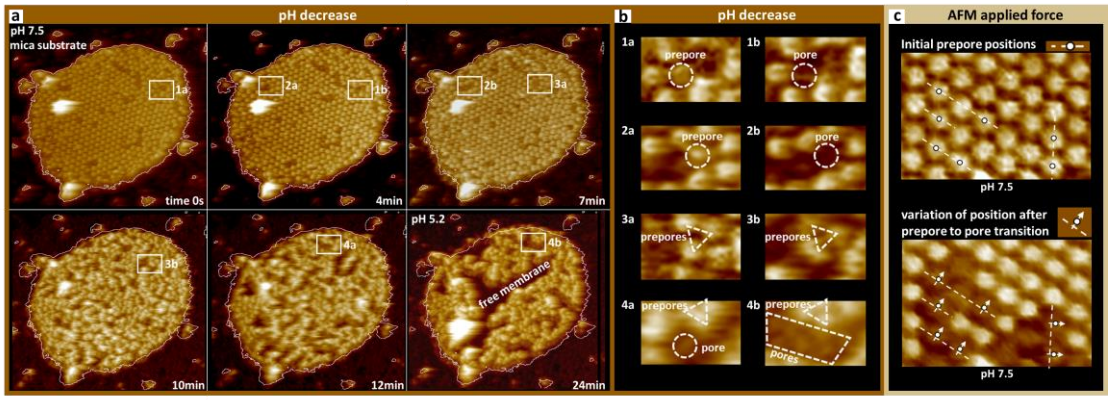

Figure 2. The prepore to pore transition increases protein-free membrane. a, six frames from Suppl. Movie 2. A patch of SM/Chol 1:1 filled by ~315 lysenin nonamers is visualized during a continuous pH decrease from 7.5 to 5.2. Image size 460nm x 460nm. The outline of patch at frame time 0s is drawn on all six frames. During the pH transition, the number of oligomers in pore state increased from 5% to 48% (~135 insertions). The area of the membrane covered by lysenin decreased by 16%, and protein-free membrane areas appeared. The total area of the patch remained unaltered. Also what we believe lipid extraction related protrusion appeared. **b**, close-up view of prepore to pore transitions, 1a to 1b and 2a to 2b; prepore configurations stable in time, 3a and 3b; and appearance of pores at pH 5.2, 4a and 4b. **c**, Single molecule compressions induced prepore-to-pore transitions in crowded lysenin assemblies at pH 7.5. After the prepore to pore transition some oligomers modify their position in the membrane, evidencing that the pores occupy less membrane area than the prepores. Help to the eye are shown in the form of lines, dots and arrows.

Preprints (www.preprints.org) | NOT PEER-REVIEWED | Posted: 5 May 2020 doi:10.20944/preprints202005.0088.v1

If prepore-to-pore transition is blocked in crowded environments and pore diameter is smaller than prepore one, we hypothesize that prepore-to-pore transition should liberate certain space that could lead to unblock other insertions. To test for the effect of liberation of space after prepore insertion, we induced prepore-to-pore transitions by a sudden decrease of pH from 7.5 to 5.2. We used a lysenin assembly incubated at 5.6μM monomer concentration and filmed the process of prepore insertions in the assembly (**Fig. 3a**), selecting five representative HS-AFM frames. For each of the five selected frames we performed cross-correlation searches to identify the position of each oligomer. We calculated the first neighbours by Delaunay triangulation. Finally, each oligomer was assigned a prepore or pore status based on the measured height. We used the list of first neighbours to identify isolated pores and lines of three consecutive pores. We named isolated pores those pores with all neighbours in the prepore state (**Fig. 3**, dashed circles). To find the lines of pores, we started with two neighbour pores and localized adjacent pores within the small arc form by connecting the centres of the oligomers (**Fig. 3**, grey ellipsoids). To cope with the complexity of crowding, we moved beyond the simple analysis of experimental images; previous analysis only based on experimental data could not detect spatially chained unblocking of the prepore-to-pore transitions [17]. We used computer simulations to generate bias-free prepore/pore neighbour statistics. Based on the list of positions of the five experimental frames we simulated prepore/pore distributions; equal probability of being a pore for all the oligomers was imposed (see five simulated frames as example in **Fig. 3b**). The percentage of pores was the same as in the experimental distributions. Next, we counted the number of isolated pores and of lines of three pores (**Fig. 3b**). We plotted the ratio of isolated pores (simulated/experimental) as a function of the percentage of pores, where we consistently observed fewer isolated pores on the experimental data than in the random simulations (**Fig. 3c**). The comparison between the experimental and simulated data show that the number of isolated pores is lower in experiments than in the simulations. Moreover, we find that it is more probable to find new pores in the vicinity of pores in the experimental data than in the simulations based on the number of isolated pores, which is higher for the simulations starting with the same number in mean. We concluded that the liberation of space after the prepore insertion is enough to unblock the prepore-to-pore transition from its steric inhibition. Experimental and simulated three pore lines ratio shows, at low pore percentages, more lines in the experimental lysenin assembly than in the simulations (**Fig. 3c**). At higher percentages we find no difference. New form pores suffer a membrane-mediated attraction toward other pores and liberate space behind, increasing insertion probability in the direction opposite to attraction; the repetition of this chain insertion mechanism create the lines of pores. The appearance of lines and not concentric circles is the result of the small diameter difference between pore and prepore, 5.5 nm^2, which does not allow the insertion of all prepore neighbours at the same time.

Preprints (www.preprints.org) | NOT PEER-REVIEWED | Posted: 5 May 2020 doi:10.20944/preprints202005.0088.v1

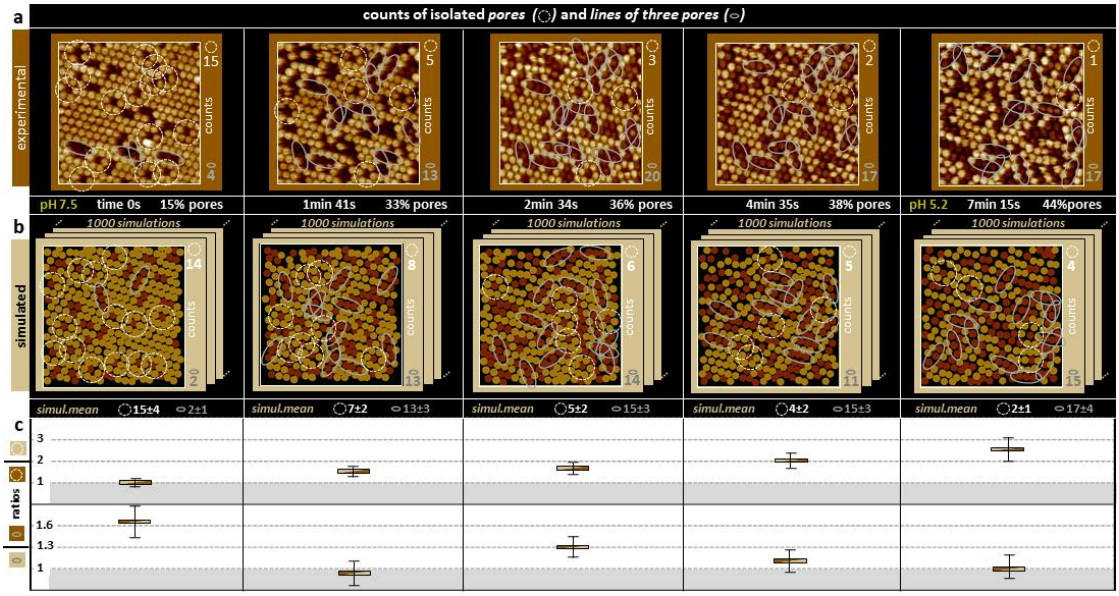

Figure 3. Evaluation of the increase of insertion probability by neighbour pores and chain insertion by comparison between experimental data and prepore and pore distribution simulations. **a**, on a lysenin oligomer hexagonal close-packed assembly we induced prepore-to-pore transitions by a pH change from 7.5 to 5.2. We observed that the percentage of pores increases as the pH decreases. Five selected HS-AFM frames with increasing percentage of pores over total number of oligomers are shown. We detected isolated pores and lines of three pores by the neighbour's analysis, highlighted in the frames. The respective counts are shown on the right side of the frame. The increase of the percentage of pores causes an increase of lines of three pores and a decrease of isolated pores. **b**, For each of the five HS-AFM experimental images simulations of randomized prepore/pore distributions are shown (1 out 1000 total). The simulations maintain the percentage of pores and the x,y positions of the oligomers. The isolated pores and lines of three pores are highlighted and the counts shown on the right side of the frame. Below, the mean counts of isolated pores and lines of three pores for the 1000 simulations is shown with its standard deviation. **c**, For different pore percentages, plots of the ratios of isolated pores and lines of three pores between the experimental data and N=1000 simulated randomized prepore/pore distributions. The probability of finding an isolated pore is less in the experimental distribution than in the random distribution, meaning that new pores appear with higher probability in the vicinity of a pore. The lower plot shows the ratio of experimental/simulated counts for the lines of three pores. In this case, it is found that in the experimental distribution is more probable to find lines of three pores than in the simulated random distribution, indicating the presence of chain insertion effect (with the exception of 33% of pores where it is equal).

Conclusions

From our study we can conclude that the steric inhibition of the prepore-to-pore transition emerge from the overall enlarge of the prepore, probably cause by the negative residues in the cytoplasmatic domain, during the invagination that results in the pore structure[18]. The actuals prepore and prepore-to-pore transition models[18],

 doi:10.20944/preprints202005.0088.v1

should be refine in order to accommodate our observations. Furthermore, the electrophysiology[9] and vesicle permeabilization experiments [20] can be now understood as a manifestation of crowding steric inhibition of pore formation. Nevertheless this work is the first direct proof of prepore enlargement structure during prepore-to-pore transition. Moreover, the prevalent appearance of pores in the borders of Lo raft-like phases show by *Yilmaz et al*.[15], can now be explain in terms of the reduction of lateral pressure on SM-rich borders which facilitates prepore insertions. Since the pores can travel in the membrane without restrictions, as shown by *Yilmaz et al*.[15]. We hypothesize that the role of the steric blockage ensures that pores are delocalized from oligomerization environment in which just prepores stay, avoiding therefore plasma membrane repair mechanisms [28 29].

Our findings highlight the importance of crowding in membranes, especially during infectious processes, and the power combining different force microscopy techniques with dedicated randomization analytical approaches to assess relevant role of crowding. We envision the steric inhibition as a new antibiotic strategy[30], using PFTs binding domains 'crowders' that would block prepore-to-pore transition, the activity of the toxin and in last term infection.

Author contributions

I.M conceived the experiments. I.M. performed the experiments. I.M., A.B. analysed the data. I.M., A.B. wrote the paper.

Acknowledgements
The authors would like to express their gratitude to Doctor Hirohide Takahashi. Others were involved in several degrees, our gratitude to all of them. Figure abstract was done by Enrique "Caik" Sainz.

References

1. Minton, A. & Wilf, J. Effect of macromolecular crowding upon the structure and function of an enzyme: glyceraldehyde-3-phosphate dehydrogenase. *Biochemistry* **20,** 4821–4826 (1981).
2. Ellis, R. J. & Minton, A. P. Cell biology: join the crowd. *Nature* **425,** 27 (2003).
3. Golkaram, M., Hellander, S., Drawert, B. & Petzold, L. R. Macromolecular crowding regulates the gene expression profile by limiting diffusion. *PLoS*

computational biology **12,** e1005122 (2016).

4. Lindén, M., Sens, P. & Phillips, R. Entropic tension in crowded membranes. *PLoS computational biology* **8,** e1002431 (2012).
5. Banerjee, P. R., Moosa, M. M. & Deniz, A. A. Two-Dimensional Crowding Uncovers a Hidden Conformation of α-Synuclein. *Angewandte Chemie International Edition* **55,** 12789–12792 (2016).
6. Guigas, G. & Weiss, M. Effects of protein crowding on membrane systems. *Biochimica et Biophysica Acta (BBA)-Biomembranes* **1858,** 2441–2450 (2016).
7. Iacovache, I., van der Goot, F. G. & Pernot, L. Pore formation: an ancient yet complex form of attack. *Biochimica et Biophysica Acta (BBA)-Biomembranes* **1778,** 1611–1623 (2008).
8. Yamaji-Hasegawa, A., Hullin-Matsuda, F., Greimel, P. & Kobayashi, T. Pore-forming toxins: Properties, diversity, and uses as tools to image sphingomyelin and ceramide phosphoethanolamine. *Biochimica et Biophysica Acta (BBA)-Biomembranes* **1858,** 576–592 (2016).
9. Krueger, E. *et al.* Intramembrane congestion effects on lysenin channel voltage-induced gating. *European Biophysics Journal* **45,** 187–194 (2016).
10. Munguira, I. *et al.* Glasslike Membrane Protein Diffusion in a Crowded Membrane. *ACS Nano* **10,** 2584–2590 (2016).
11. Abrami, L. & Van Der Goot, F. G. Plasma membrane microdomains act as concentration platforms to facilitate intoxication by aerolysin. *The Journal of cell biology* **147,** 175–184 (1999).
12. Lafont, F. & Van Der Goot, F. G. Bacterial invasion via lipid rafts. *Cellular*

 doi:10.20944/preprints202005.0088.v1

microbiology **7,** 613–620 (2005).

13. SEKIZAWA, Y., HAGIWARA, K., NAKAJIMA, T. & KOBAYASHI, H. A novel protein, lysenin, that causes contraction of the isolated rat aorta: its purification from the coelomic fluid of the earthworm, Eisenia foetida. *Biomedical Research* **17,** 197–203 (1996).

14. Yilmaz, N. *et al.* Real-time visualization of assembling of a sphingomyelin-specific toxin on planar lipid membranes. *Biophysical journal* **105,** 1397–1405 (2013).

15. Yilmaz, N. & Kobayashi, T. Visualization of lipid membrane reorganization induced by a pore-forming toxin using high-speed atomic force microscopy. *ACS nano* **9,** 7960–7967 (2015).

16. Ishitsuka, R. & Kobayashi, T. Cholesterol and lipid/protein ratio control the oligomerization of a sphingomyelin-specific toxin, lysenin. *Biochemistry* **46,** 1495–1502 (2007).

17. Munguira, I. L. B., Takahashi, H., Casuso, I. & Scheuring, S. Lysenin Toxin Membrane Insertion Is pH-Dependent but Independent of Neighboring Lysenins. *Biophysical Journal* **113,** 2029–2036 (2017).

18. Podobnik, M. *et al.* Crystal structure of an invertebrate cytolysin pore reveals unique properties and mechanism of assembly. *Nature communications* **7,** 11598 (2016).

19. Bokori-Brown, M. *et al.* Cryo-EM structure of lysenin pore elucidates membrane insertion by an aerolysin family protein. *Nature communications* **7,** 11293 (2016).

 doi:10.20944/preprints202005.0088.v1

20. Alam, J. M., Kobayashi, T. & Yamazaki, M. The single-giant unilamellar vesicle method reveals lysenin-induced pore formation in lipid membranes containing sphingomyelin. *Biochemistry* **51,** 5160–5172 (2012).

21. Ando, T. *et al.* A high-speed atomic force microscope for studying biological macromolecules. *Proceedings of the National Academy of Sciences* **98,** 12468–12472 (2001).

22. Simons, K. & Gerl, M. J. Revitalizing membrane rafts: new tools and insights. *Nature reviews Molecular cell biology* **11,** nrm2977 (2010).

23. Goncalves, R. P. *et al.* Two-chamber AFM: probing membrane proteins separating two aqueous compartments. *Nature methods* **3,** 1007 (2006).

24. Reviakine, I., Bergsma-Schutter, W. & Brisson, A. Growth of Protein 2-D Crystals on Supported Planar Lipid Bilayers Imagedin Situby AFM. *Journal of structural biology* **121,** 356–362 (1998).

25. Kobayashi, H., Ohtomi, M., Sekizawa, Y. & Ohta, N. Toxicity of coelomic fluid of the earthworm Eisenia foetida to vertebrates but not invertebrates: probable role of sphingomyelin. *Comparative Biochemistry and Physiology Part C: Toxicology & Pharmacology* **128,** 401–411 (2001).

26. Leung, C. *et al.* Stepwise visualization of membrane pore formation by suilysin, a bacterial cholesterol-dependent cytolysin. *elife* **3,** (2014).

27. Czajkowsky, D. M., Sun, J., Shen, Y. & Shao, Z. Single molecule compression reveals intra-protein forces drive cytotoxin pore formation. *eLife Sciences* **4,** e08421 (2015).

28. Bischofberger, M. & Iacovache, I. Pathogenic pore-forming proteins:

 doi:10.20944/preprints202005.0088.v1

function and host response. *Cell host & microbe* **12,** 266–275 (2012).

29. Aroian, R. & van der Goot, F. G. Pore-forming toxins and cellular non-immune defenses (CNIDs). *Current Opinion in Microbiology* **1,** 57–61 (2007).

30. Hu, C.-M. J., Fang, R. H., Copp, J., Luk, B. T. & Zhang, L. A biomimetic nanosponge that absorbs pore-forming toxins. *Nature nanotechnology* **8,** 336 (2013).

31. Hancock, R. E. & Sahl, H.-G. Antimicrobial and host-defense peptides as new anti-infective therapeutic strategies. *Nature biotechnology* **24,** 1551 (2006).

32. Zuttion, F., Redondo-Morata, L., Marchesi, A. & Casuso, I. High-Resolution and High-Speed Atomic Force Microscope Imaging. in *Nanoscale Imaging* 181–200 (Humana Press, New York, NY, 2018). doi:10.1007/978-1-4939-8591-3_11